Available online at www.sciencedirect.com
SCIENCE DIRECT®
Journal of Sound and Vibration 289 (2006) 360–381
JOURNAL OF SOUND AND VIBRATION
www.elsevier.com/locate/jsvi

Nonlinear dynamic analysis of rolling element bearings due to cage run-out and number of balls

S.P. Harsha*

Mechanical Engineering Group, Birla Institute of Technology & Science, Pilani 333031, India

Received 28 July 2003; received in revised form 24 May 2004; accepted 8 February 2005
Available online 27 April 2005

Abstract

This paper presents an analytical model to investigate the nonlinear dynamic behavior due to cage run-out and number of balls in a rotating system supported by rolling element bearings. Due to run-out of the cage, the rolling elements no longer stay equally spaced. The mathematical model takes into account the sources of nonlinearity such as the Hertzian contact force and cage run-out resulting transition from no contact to contact state between rolling elements and races. The contact between the rolling elements and races is treated as nonlinear springs. The nonlinear stiffness is obtained by application of Hertzian contact deformation theory. The implicit-type numerical integration technique Newmark-β with Newton–Raphson method is used to solve the nonlinear differential equations iteratively. The results are presented in the form of fast Fourier transformations (FFT) and phase trajectories. It is implied from the obtained FFT that due to the non-uniform spacing the ball passage frequency is modulated with the cage frequency.

1. Introduction

An analysis of ball-bearing dynamic behavior is important to predict the system vibration responses. The behavior of nonlinear systems often demonstrates unexpected behavior patterns that are extremely sensitive to initial conditions. Many advanced bearing applications now require understanding of dynamic effects and classical quasi-static analysis techniques of Jones [1], Harris

*Tel.: +91 01596 242210; fax: +91 01596 244183.
E-mail address: spharsha@yahoo.com.

0022-460X/$ - see front matter © 2005 Elsevier Ltd. All rights reserved.
doi:10.1016/j.jsv.2005.02.021

Nomenclature

F_u	unbalance force, N
I	moment of inertia of each rolling element
I_{shaft}	moment of inertia of the shaft
I_{in}	moment of inertia of the inner race
I_{out}	moment of inertia of the outer race
k	waviness order
K	constant of proportionality, N/mm
M_c	mass of the cage, kg
m_{in}	mass of the inner race, kg
m_j	mass of the rolling elements, kg
m_{out}	mass of the outer race, kg
N_b	number of balls
p	empirical constant for a particular geometry
q	empirical constant for a particular geometry
R	radius of outer race, mm
r	radius of inner race, mm
r_{in}	position of mass center of inner race
r_{out}	position of mass center of outer race
T	kinetic energy of the bearing system
T_{cage}	kinetic energy of the cage
$T_{\text{i\_race}}$	kinetic energy of the inner race
$T_{\text{o\_race}}$	kinetic energy of the outer race
$T_{\text{r.e.}}$	kinetic energy of the rolling elements
V	potential energy of the bearing system
V_{cage}	potential energy of the cage
$V_{\text{i\_race}}$	potential energy of the inner race
$V_{\text{o\_race}}$	potential energy of the outer race
$V_{\text{r.e.}}$	potential energy of the rolling elements
V_{spring}	potential energy of the springs
$x_{\text{in}}, y_{\text{in}}$	center of inner race
$x_{\text{out}}, y_{\text{out}}$	center of outer race
δ	deformation at the point of contact at inner and outer race, mm
Γ	small run-out of cage, μm
$(\dot{\phi})_{\text{in}}$	angular velocity of inner race
$(\dot{\phi})_{\text{out}}$	angular velocity of outer race
ω_c	angular velocity of cage relating to the cage, rad/s
ω_{bp}	ball passage frequency, Hz
ρ_j	radial position of the rolling element
ρ_r	radius of each rolling element
θ_j	angular position of rolling element
χ_j	position of jth rolling element from the center of inner race
FFT	fast Fourier transformation

[2], Palmgren [3]; others are inadequate for dynamic analysis. Cage failures due to high pocket wear or destructive collision forces between the cage and rolling element or race lands, cage-induced audio noise and structural vibration and excessive torque or torque noise are examples of bearing performance characteristics that are significantly affected by dynamics. Ball-to-ball cage interactions can induce excessive ball to race skidding and degraded performance and can cause premature failure. When ball bearings are operated at high speed, they generate vibrations and noise. The principle forces, which drive these vibrations, are time-varying nonlinear contact forces, which exist between the various components of the bearings: balls, races and shafts. Since today, ball bearings are used in the design of increasingly sophisticated arrangements, involving high speeds, high temperature, heavy or unusual loading and requiring continuous operations, automation etc.; a clear understanding of vibrations associated with them is needed. It is generally accepted that it is impossible to produce a perfect surface or contour even with the best machine tools and this applies also to ball-bearing manufacturing. In the shaft-bearing assembly supported by perfect ball bearings, the vibration spectrum is dominated by the vibrations at the natural frequency and the ball passage frequency (BPF). The vibrations at this later frequency are called ball passage vibrations (BPV).

Walters [4] developed an analytical model for ball bearing and cage dynamics with ball raceway slip that was later modified by Gupta [5,6]. However, the solution of time-varying Hertzian contact stress for each ball, along with integration of each cage impact with the balls or raceways and integration of the ball traction/slip forces at each contact point on the inside and outside raceways, results in long computer run times and can be so costly as to make parametric design studies impractical. In addition, the Walters/Gupta model equations are written in the fixed inertial coordinate system that leads to complex equations of motion, excessively long computer times and computational errors due to computer numerical truncation. Kennel and Bupara [7] developed a simplified method for analyzing ball and cage dynamics and they assumed that the ball cage is only to move in the plane of its major diameter. Meeks et al. [8,9] have shown that the ball cage motions are far too complex to be modeled with this extreme simplification of cage motion. Meeks and Tran [10] developed an analytical model to study and optimize the bearing and cage design parameters. Gad et al. [11] showed that resonance occurs when BPF coincides with frequency of the system and they also pointed out that for certain speeds, BPF can exhibit its sub- and super-harmonic vibrations for the shaft-ball-bearing system. Rahnejat and Gohar [12] showed that even in the presence of elastohydrodynamic lubricating film between balls and the races, a peak at the BPF appears in the spectrum. Aktürk et al. [13] performed a theoretical investigation of the effect of varying the preload on the vibration characteristics of a shaft-bearing system and also suggested that by taking correct number of balls and amount of preload in a bearing untoward effect of the BPV can be reduced.

Harsha et al. [14] developed an analytical model to predict nonlinear dynamic response in a rotor-bearing system due to surface waviness. The conclusion of this work shows that for the *outer race waviness*, the severe vibrations occur when the number of balls and waves are equal. In case of the *inner race waviness*, the peak amplitude of vibration can be at $q\omega_{\mathrm{wp}} \pm p\omega_{\mathrm{cage}}$. For the waviness order iN_b, peak amplitude of vibration and super-harmonic appear at the wave passage speed (ω_{wp}). Harsha et al. [15] analyzed the nonlinear behaviors of ball bearing due to number of balls and preload effect. Nonlinear dynamic response is found to be associated with the BPF. The amplitude of the vibration is considerably reduced if the number of balls and preload are correctly selected. Harsha et al. [16] analyzed the nonlinear behaviors of the high-speed horizontal balanced rotor supported by ball bearings. The conclusion of this work shows that most severe vibrations occur when the BPF and its harmonics coincide with the natural frequency. Harsha [17] analyzed the stability analysis of the rotor-bearing system. In the analytical formulation the contacts between the balls and races are considered as nonlinear springs, whose stiffness is obtained by using the Hertzian elastic contact deformation theory. The appearance of regions of periodic, sub-harmonic and chaotic behavior is seen to be strongly dependent on the radial internal clearance and rotor speed. Poincaré maps and frequency spectra are used to elucidate and to illustrate the diversity of the system behavior.

In this paper, theoretical investigation was made to observe the effect of cage run-out and number of balls on the vibration characteristics of the ball-bearing system. The system was considered with the assumption that there is no friction between the rolling elements and raceways. In terms of the feature that the nonlinear bearing forces act on the system, the implicit-type numerical integration technique Newmark-β [18] with the Newton–Raphson method is used to solve the nonlinear differential equations iteratively. The integration is needed at each step of integrations to execute only on small parts of the system equations related to the nonlinear terms.

The results obtained from a large number of numerical integrations are mainly presented in form of FFT and phase plots.

2. The problem formulation

A schematic diagram of rolling element bearing is shown in Fig. 1. For investigating the structural vibration characteristics of rolling element bearing, a model of bearing assembly can be considered as a spring-mass system, in which the outer race of the bearing is fixed in a rigid support and the inner race is fixed rigidly with the shaft. Elastic deformation between races and rollers give a nonlinear force deformation relation, which is obtained by the Hertzian theory. Other sources of stiffness variation are positive internal radial clearance, finite number of balls whose position changes periodically and the inner and outer race waviness. These cause periodic changes in stiffness of bearing assembly. Thus, the system undergoes nonlinear vibration under dynamic conditions.

In the mathematical modeling, the rolling element bearing is considered as the spring-mass system and rolling elements act as a nonlinear contact spring as a shown in Fig. 2. Since, the Hertzian forces arise only when there is contact deformation, the springs are required to act only in compression. In other words, the respective spring force comes into play when the instantaneous spring length is shorter than its unstressed length, otherwise the separation between the rolling element and the races takes place and the resultant force is set to zero.

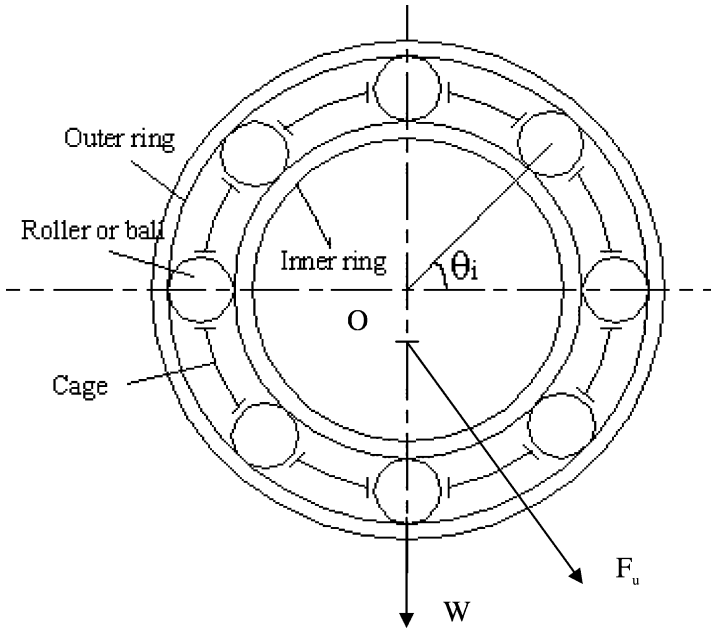

Fig. 1. A schematic diagram of a rolling element bearing.

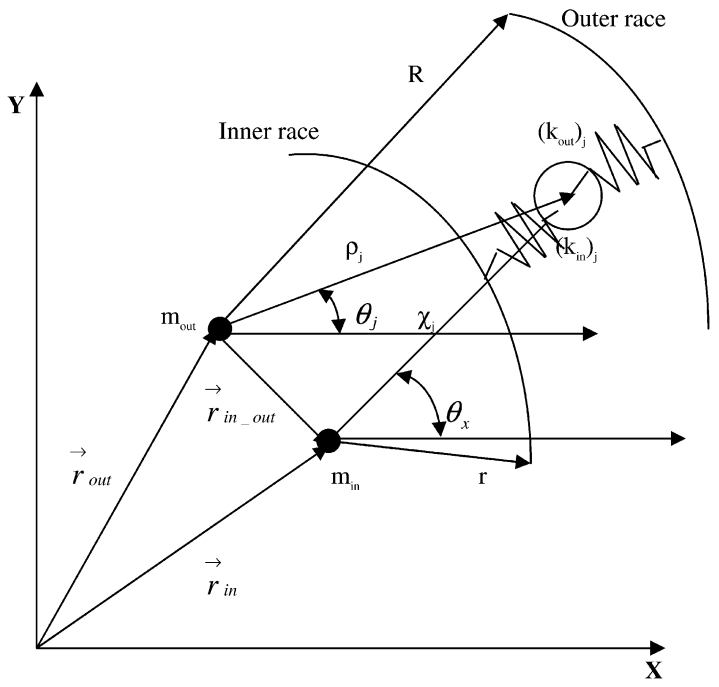

Fig. 2. Mass-spring model of the rolling element bearing.

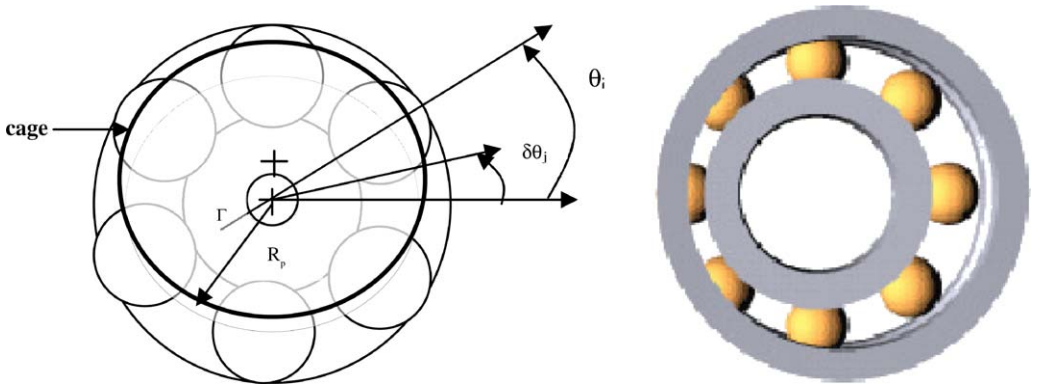

Fig. 3. Non-uniform ball spacing due to cage run-out.

2.1. Cage run-out

Due to the run-out of the cage, the rolling elements no longer stay equally spaced, as shown in Fig. 3. The resulting variations of the circumferential angle for a small run-out (Γ) is

$$\delta\theta_j = \frac{\Gamma}{R_p}\cos(\theta_j), \tag{1}$$

where R_p denotes the pitch radius.

Due to the non-uniform spacing, the BPF is modulated with the cage frequency. The angular excitation frequencies due to the cage run-out are given by

$$\omega = q\omega_{\mathrm{bp}} \pm k\omega_c. \tag{2}$$

2.2. Contact stiffness

Hertz considered the stress and deformation in the perfectly smooth, ellipsoidal, contacting elastic solids. The application of the classical theory of elasticity to the problem forms the basis of stress calculation for machine elements as ball and roller bearings. Therefore, the point contact between the race and ball develops into an area contact, which has the shape of an ellipse with a and b as the semi-major and semi-minor axes, respectively. The curvature sum and difference are needed in order to obtain the contact force of the ball. The curvature sum $\sum \rho$ as obtained from Harris [2] is expressed as

$$\sum \rho = \rho_{\mathrm{I1}} + \rho_{\mathrm{I2}} + \rho_{\mathrm{II1}} + \rho_{\mathrm{II2}} = \frac{1}{r_{\mathrm{I1}}} + \frac{1}{r_{\mathrm{I2}}} + \frac{1}{r_{\mathrm{II1}}} + \frac{1}{r_{\mathrm{II2}}}. \tag{3}$$

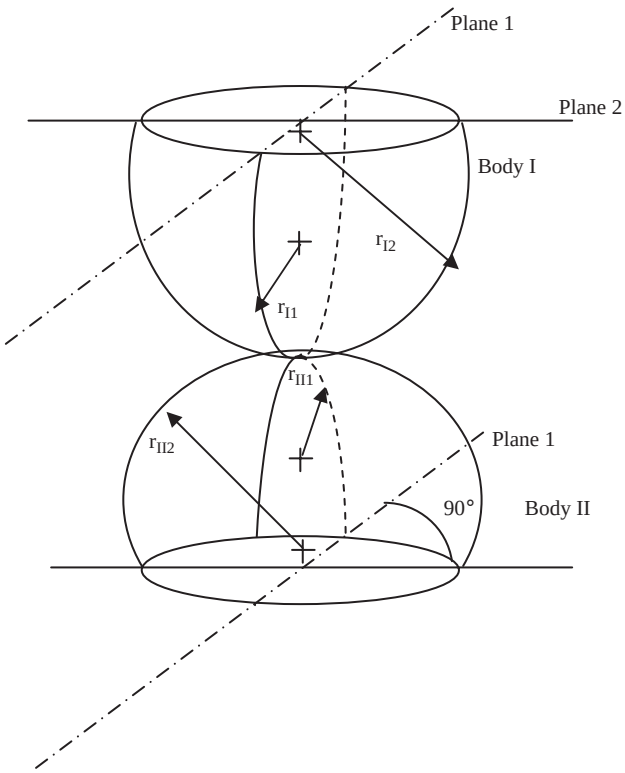

Fig. 4. Geometry of contacting bodies.

The curvature difference $F(\rho)$ is expressed as

$$F(\rho) = \frac{(\rho_{I1} - \rho_{I2}) + (\rho_{II1} - \rho_{II2})}{\sum \rho}. \tag{4}$$

The parameters $r_{I1}, r_{I2}, r_{II1}, r_{II2}, \rho_{I1}, \rho_{I2}, \rho_{II1}, \rho_{II2}$ are given dependent upon calculations referring to the inner and outer races as shown in Fig. 4. If the inner race is considered,

$$r_{I1} = D/2, \quad r_{I2} = D/2, \quad r_{II1} = d/2, \quad r_{II2} = r$$

and

$$\rho_{I1} = 2/D, \quad \rho_{I2} = 2/D, \quad \rho_{II1} = 2/d, \quad \rho_{II2} = -1/r. \tag{5}$$

If the outer race is considered, they are given as

$$r_{I1} = D/2, \quad r_{I2} = D/2, \quad r_{II1} = D/2, \quad r_{II2} = R$$

and

$$\rho_{I1} = 2/D, \quad \rho_{I2} = 2/D, \quad \rho_{II1} = -2/D, \quad \rho_{II2} = -1/R. \tag{6}$$

As per the sign convention followed, negative radius denotes a concave surface. Using Table 2 calculation of all the parameters including curvature difference at inner and outer race can be done. For the contacting bodies made of steel, the relative approach between two contacting and deforming surfaces is given by

$$\delta = 2.787 \times 10^{-8} Q^{2/3} \left(\sum \rho\right)^{1/3} \delta^*, \tag{7}$$

where δ^* is a function of $F(\rho)$.

Hence, the contact force (Q) is

$$Q = \left\{(3.587 \times 10^7)^{3/2} \left(\sum \rho\right)^{-1/2} (\delta^*)^{-3/2}\right\} \delta^{3/2} \quad \text{(N)}. \tag{8}$$

The elastic modulus for the contact of a ball with the inner race is

$$K_i = \frac{Q}{\delta_{in}} = (3.587 \times 10^7)^{3/2} \left(\sum \rho_i\right)^{-1/2} (\delta_i^*)^{-3/2} (\delta)^{1/2} \quad \text{(N/mm)}. \tag{9}$$

And for the contact of a ball with the outer race it is

$$K_o = \frac{Q}{\delta_{out}} = (3.587 \times 10^7)^{3/2} \left(\sum \rho_o\right)^{-1/2} (\delta_o^*)^{-3/2} (\delta)^{1/2} \quad \text{(N/mm)}. \tag{10}$$

Then the effective elastic modulus K for the bearing system is written as

$$K = \frac{1}{(1/K_i^{1/n} + 1/K_o^{1/n})^n}. \tag{11}$$

In Eqs. (8) and (9), the parameters δ_i^* and δ_o^* can be attained from Table 1, if the values of $F(\rho)_i$ and $F(\rho)_o$ are available using Table 2. The effective elastic modulus (K) for the bearing system

Table 1
Dimensional contact parameters [2]

$F(\rho)$	δ
0	1
0.1075	0.997
0.3204	0.9761
0.4795	0.9429
0.5916	0.9077
0.6716	0.8733
0.7332	0.8394
0.7948	0.7961
0.83595	0.7602
0.87366	0.7169
0.90999	0.6636
0.93657	0.6112
0.95738	0.5551
0.97290	0.4960
0.983797	0.4352
0.990902	0.3745
0.995112	3176
0.997300	0.2705
0.9981847	0.2427
0.9989156	0.2106
0.9994785	0.17167
0.9998527	0.11995
1	0

Table 2
Geometric and physical properties used for the rolling element bearings

Mass of rolling element (m_j)	0.024 kg
Mass of the inner race (m_{in})	0.06 kg
Mass of the outer race (m_{out})	0.065 kg
Mass of the shaft (m_c)	0.009 kg
Diameter of inner race with point of contact with the rolling element ($2r$)	18.738 mm
Diameter of outer race with point of contact with the rolling element ($2R$)	28.262 mm
Ball diameter (D)	4.762 mm
Radial load (W)	24 N
Angular velocity of inner race	5000 rev/min
Cage run-out (Γ)	0.01 μm
Initial radial position of jth rolling element (ρ_j)	27 mm
Initial position of center of inner race (x_{in}, y_{in})	(0, 0) mm
Initial position of center of inner race (x_{out}, y_{out})	(0, 0) mm

using geometrical and physical parameters is written as

$$K = 7.055 \times 10^5 \sqrt{\delta} \quad (\mathrm{N/mm}). \tag{12}$$

2.3. Derivation of governing equations of motion

A real rotor-bearing system is generally very complicated and difficult to model; so for an effective and simplified mathematical model the following assumptions are made:

1. Deformations occur according to the Hertzian theory of elasticity. Small elastic motions of the rolling elements and the rings are considered but plastic deformations are neglected.
2. The rolling elements, the inner and outer races and the rotor have motions in the plane of bearing only.
3. The angular velocity of the cage is assumed to be constant.
4. The rollers in a rolling element bearing are assumed to have no angular rotation about their axes, i.e. no skewing. Hence, there is no interaction of the corners of the rollers with the cage and the flanges of the races.
5. All the bearing components and the rotor are rigid, i.e. there is no bending.
6. The bearings are assumed to operate under isothermal conditions. Hence, all thermal effects that may arise due to the rise in temperature, such as change of lubricant viscosity, expansion of the rolling elements and the races and reduction of endurance of the material, are considered absent.
7. There is no slipping of balls as they roll on the surface of races. Since there is perfect rolling of the balls on the surface of races and the two points of ball touching the races have different linear velocities, the center of the ball has a resultant translational velocity.
8. The damping of a ball bearing is very small. This damping is present because of friction and small amount of lubrication. The estimation of damping of ball bearing is very difficult because of the dominant extraneous damping that swamps the damping of the bearing.
9. The cage ensures the constant angular separation (β) between rolling elements; hence there is no interaction between rolling elements. In addition, at any given instant, some of the rolling elements will contact both races. Hence,

$$\beta = \frac{2\pi}{N_b}. \tag{13}$$

The equations of motion that describe the dynamic behavior of the complete model can be derived by using Lagrange's equation for a set of independent generalized coordinates as

$$\frac{\mathrm{d}}{\mathrm{d}t}\frac{\partial T}{\partial \{\dot{p}\}} - \frac{\partial T}{\partial \{p\}} + \frac{\partial V}{\partial \{p\}} = \{f\}, \tag{14}$$

where T, V, p and f are kinetic energy, potential energy, vector with generalized degree-of-freedom (dof) coordinate and vector with generalized contact forces, respectively. The kinetic and potential energies can be subdivided into the contributions from the various components, i.e. from the rolling elements, the inner race, the outer race and the rotor.

The total kinetic energy (T) of the rotor-bearing system is the sum of the rolling elements, inner and outer races and the rotor:

$$T = T_{\text{r.e.}} + T_{\text{i\_race}} + T_{\text{o\_race}} + T_{\text{cage}}. \tag{15}$$

The subscripts i_race, o_race and cage refer to, respectively, the inner race, the outer race and the cage. The subscript r.e. indicates the rolling elements.

The potential energy is provided by deformations of the balls with the races and deformations occur according to the Hertzian contact theory of elasticity. Potential energy formulation is performed taking datum as the horizontal plane through the global origin. The total potential energy (V) of the bearing system is the sum of the balls, inner and outer races, springs and the rotor:

$$V = V_{\text{r.e.}} + V_{\text{i\_race}} + V_{\text{o\_race}} + V_{\text{springs}} + V_{\text{cage}}, \tag{16}$$

where $V_{\text{r.e.}}$, $V_{\text{i\_race}}$, $V_{\text{o\_race}}$ and V_{cage} are the potential energies due to elevation of the rolling elements, inner and outer races and the rotor, respectively. V_{springs} is the potential energy due to nonlinear spring contacts between rollers and the races.

2.3.1. Contribution of the inner race

Apart from local deformations in the contacts, the inner race is considered as a rigid body. The kinetic energy of the inner race about its center of mass is evaluated in x- and y-frame. The position of the origin of the moving frame relative to the reference frame is described by transitional dof $\dot{x}_{\text{in}}$ and $\dot{y}_{\text{in}}$.

The kinetic energy expression for the inner race is

$$T_{\text{i\_race}} = \tfrac{1}{2} m_{\text{in}} (\dot{\vec{r}}_{\text{in}} \bullet \dot{\vec{r}}_{\text{in}}) + \tfrac{1}{2} I_{\text{in}} \dot{\phi}_{\text{in}}^2. \tag{17}$$

The displacement vector showing the location of the inner race center with respect to that of the outer race center is then given by

$$\vec{r}_{\text{in}} = \vec{r}_{\text{out}} + \vec{r}_{\text{in\_out}} \tag{18}$$

or

$$\vec{r}_{\text{in}} = (\vec{x}_{\text{in}} + \vec{x}_{\text{out}})\hat{i} + (\vec{y}_{\text{in}} + \vec{y}_{\text{out}})\hat{j}. \tag{19}$$

Differentiating r_{in} with respect to time (t) and putting that value in Eq. (17) gives

$$T_{\text{i\_race}} = \tfrac{1}{2} m_{\text{in}} \left(\dot{x}_{\text{in}}^2 + \dot{y}_{\text{in}}^2 \right) + \tfrac{1}{2} I_{\text{in}} \dot{\phi}_{\text{in}}^2. \tag{20}$$

Since the position of the inner race is defined from the outer race center, the potential energy for the inner race is

$$V_{\text{i\_race}} = m_{\text{in}} g (y_{\text{in\_out}} + y_{\text{out}}). \tag{21}$$

2.3.2. Contribution of the outer race

The outer race is also considered as a rigid body and it is assumed that the outer race is stationary. Hence, $\dot{r}_{\text{out}} = 0$ and $\dot{\phi}_{\text{out}} = 0$. The kinetic energy expression for the outer race is zero.

The potential energy of the outer race is

$$V_{\text{o\_race}} = m_{\text{out}} g y_{\text{out}}. \tag{22}$$

2.3.3. Contribution of the rolling elements

The rolling elements are also considered as rigid bodies. For the determination of their contribution to the kinetic energy, the position of the jth-rolling element is described by two transitional dof,

$$(\dot{\rho}_j + \dot{r}_{\text{out}}) \quad \text{and} \quad \dot{\phi}_j.$$

The kinetic energy due to rolling elements obtained as a summation of those from each element is

$$T_{\text{r.e.}} = \sum_{j=1}^{N_b} T_j. \tag{23}$$

The position of the center of roller is defined with respect to the outer race center. Hence, the kinetic energy of the rolling elements may be written as

$$T_j = \tfrac{1}{2} m_j \left(\dot{\vec{\rho}}_j + \dot{\vec{r}}_{\text{out}}\right) \bullet \left(\dot{\vec{\rho}}_j + \dot{\vec{r}}_{\text{out}}\right) + \tfrac{1}{2} I_j \dot{\phi}_j^2. \tag{24}$$

The displacement vector showing the location of jth rolling elements is

$$\vec{\rho}_j = (\vec{\rho}_j \cos\theta_j)\hat{i} + (\vec{\rho}_j \sin\theta_j)\hat{j}. \tag{25}$$

And for the outer race center it is

$$\vec{r}_{\text{out}} = \vec{x}_{\text{out}}\hat{i} + \vec{y}_{\text{out}}\hat{j}. \tag{26}$$

The summation of Eqs. (25) and (26) after differentiation with respect to time (t) leads to the following expression:

$$\begin{aligned}\left(\dot{\vec{\rho}}_j + \dot{\vec{r}}_{\text{out}}\right) \bullet \left(\dot{\vec{\rho}}_j + \dot{\vec{r}}_{\text{out}}\right) = {} & \dot{\rho}_j^2 \cos^2\theta_j + \rho_j^2 \sin^2\theta_j \cdot \dot{\theta}_j^2 - 2\dot{\rho}_j \cdot \rho_j \cdot \dot{\theta}_j \cos\theta_j \sin\theta_j \\ & + \dot{x}_{\text{out}}^2 + 2\dot{x}_{\text{out}}(\dot{\rho}_j \cos\theta_j - \rho_j \sin\theta_j \cdot \dot{\theta}_j) + \dot{\rho}_j^2 \sin^2\theta_j \\ & + \rho_j^2 \cos^2\theta_j \cdot \dot{\theta}_j^2 + 2\dot{\rho}_j \cdot \rho_j \cdot \dot{\theta}_j \cos\theta_j \sin\theta_j \\ & + \dot{y}_{\text{out}}^2 + 2\dot{y}_{\text{out}}(\dot{\rho}_j \cos\theta_j - \rho_j \sin\theta_j \cdot \dot{\theta}_j).\end{aligned} \tag{27}$$

The outer race is assumed to be stationary; hence $\dot{x}_{\text{out}} = 0$ and $\dot{y}_{\text{out}} = 0$. Therefore, Eq. (27) becomes

$$\left(\dot{\vec{\rho}}_j + \dot{\vec{r}}_{\text{out}}\right) \bullet \left(\dot{\vec{\rho}}_j + \dot{\vec{r}}_{\text{out}}\right) = \dot{\rho}_j^2 \cos^2\theta_j + \rho_j^2 \sin^2\theta_j \cdot \dot{\theta}_j^2 + \dot{\rho}_j^2 \sin^2\theta_j + \rho_j^2 \cos^2\theta_j \cdot \dot{\theta}_j^2 \tag{28}$$

or

$$\left(\dot{\vec{\rho}}_j + \dot{\vec{r}}_{\text{out}}\right) \bullet \left(\dot{\vec{\rho}}_j + \dot{\vec{r}}_{\text{out}}\right) = \left(\dot{\rho}_j^2 + \rho_j^2 \cdot \dot{\theta}_j^2\right). \tag{29}$$

From Eq. (24), we get

$$T_j = \tfrac{1}{2} m_j \left(\dot{\rho}_j^2 + \rho_j^2 \cdot \dot{\theta}_j^2\right) + \tfrac{1}{2} I_j \dot{\phi}_j^2. \tag{30}$$

It is assumed that there is no slip; hence, the relative transitional velocity of the outer race and rolling element must be the same and in opposite direction. Therefore, the contact equation for the jth rolling element and the outer race can be written as

$$R\left(\dot{\phi}_{\text{out}} - \dot{\theta}_j\right) = -\rho_r \left(\dot{\phi}_j - \dot{\theta}_j\right). \tag{31}$$

Since the outer race is stationary,

$$\dot{\phi}_{\text{out}} = 0. \tag{32}$$

The rotation of the jth rolling element about its center of mass is

$$\dot{\phi}_j = \dot{\theta}_j \left(1 + \frac{R}{\rho_r}\right). \tag{33}$$

Now the kinetic energy of the rolling elements can be written as

$$T_{\text{r.e.}} = \sum_{j=1}^{N_b} \frac{1}{2} m_j \left(\dot{\rho}_j^2 + \rho_j^2 . \dot{\theta}_j^2\right) + \frac{1}{2} I_j \dot{\theta}_j^2 \left(1 + \frac{R}{\rho_r}\right)^2. \tag{34}$$

The position of the center of roller is defined with respect to the outer race center. Hence, the potential energy of the rolling elements may be written as

$$V_{\text{r.e.}} = \sum_{j=1}^{N_b} m_j g(\rho_j \sin\theta_j + y_{\text{out}}) \tag{35}$$

or

$$V_{\text{r.e.}} = mgN_b y_{\text{out}} + \sum_{j=1}^{N_b} (m_j g \rho_j \sin\theta_j). \tag{36}$$

2.3.4. Contribution of the cage

The kinetic energy of the cage is calculated by assuming that its center remains coincident with the inner race. Hence, the kinetic energy of the cage is

$$T_{\text{cage}} = \tfrac{1}{2} m_c \left(\dot{x}_{\text{in}}^2 + \dot{y}_{\text{in}}^2\right) + \tfrac{1}{2} I_c \dot{\theta}_c^2. \tag{37}$$

The cage center coincides with the inner race center and the position of the inner race center is defined with respect to the outer race center. Hence, the potential energy of the cage is expressed as

$$V_{\text{cage}} = m_c g(y_{\text{in\_out}} + y_{\text{out}}). \tag{38}$$

2.3.5. Contribution of the contact deformation

The contacts between balls and races are treated as nonlinear springs, whose stiffness is obtained by the Hertzian theory of elasticity. The expression of potential energy due to the contact deformation of the springs is

$$V_{\text{spring}} = \sum_{j=1}^{N_b} \frac{1}{2} k_{\text{in}} \delta_{\text{in}}^2 + \sum_{j=1}^{N_b} \frac{1}{2} k_{\text{out}} \delta_{\text{out}}^2, \tag{39}$$

where k_{in} and k_{out} are the nonlinear stiffness due to Hertzian contact effects.

The deformation at contact points between the jth rolling element and inner race is

$$\delta_{\text{in}} = [\{r + \rho_r + \Gamma\} - \chi_j]. \tag{40}$$

In this expression, if $\{r + \rho_r + \Gamma\} > \chi_j$, compression takes place and restoring force acts.

If $\{r + \rho_r + \Gamma\} < \chi_j$, no compression and restoring force is set to zero.

Similarly, at the outer race the deformation at the contact points is

$$\delta_{\text{out}} = [R - \{\rho_j + \rho_r + \Gamma\}]. \tag{41}$$

In this expression, if $R < \{\rho_j + \rho_r + \Gamma\}$, compression takes place and restoring force acts.

If $R > \{\rho_j + \rho_r + \Gamma\}$, no compression and restoring force is set to zero.

2.4. Equations of motion

The kinetic energy and potential energy contributed by the inner race, outer race, balls, shaft and springs can be differentiated with respect to the generalized coordinates ρ_j ($j = 1, 2, \ldots, N_b$), x_{in}, and y_{in} to obtain the equations of motion. For the generalized coordinates ρ_j, where $j = 1, 2, \ldots, N_b$, the equations are

$$\begin{aligned} m_j \ddot{\rho}_j + m_j g \sin\theta_j + m_j \rho_j \dot{\theta}^2 - (k_{\text{in}})[(r + \rho_r + \Gamma) - \chi_j]_+ \frac{\partial \chi_j}{\partial \rho_j} + (k_{\text{out}})[R - (\rho_j + \rho_r + \Gamma)]_+ \\ + \frac{1}{2} \frac{\partial k_{\text{in}}}{\partial \rho_j} [(r + \rho_r + \Gamma) - \chi_j]_+^2 + \frac{1}{2} \frac{\partial k_{\text{out}}}{\partial \rho_j} [R - (\rho_j + \rho_r + \Gamma)]_+^2 = 0, \quad j = 1, 2, \ldots, N_b. \end{aligned} \tag{42}$$

For the generalized coordinate x_{in} the equation is

$$(m_{\text{in}} + m_c)\ddot{x}_{\text{in}} - \sum_{j=1}^{N_b} k_{\text{in}}[(r + \rho_r + \Gamma) - \chi_j]_+ \frac{\partial \chi_j}{\partial x_{\text{in}}} = F_u \sin(\omega t). \tag{43}$$

For the generalized coordinate y_{in} the equation is

$$(m_{\text{in}} + m_c)\ddot{y}_{\text{in}} + (m_{\text{in}} + m_c)g - \sum_{j=1}^{N_b} k_{\text{in}}[(r + \rho_r + \Gamma) - \chi_j]_+ \frac{\partial \chi_j}{\partial y_{\text{in}}} = W + F_u \cos(\omega t). \tag{44}$$

This is a system of $(N_b + 2)$ second-order, nonlinear differential equations. There is an external radial force allowed to act on the bearing system and no external mass is attached to the outer race. The "+" sign as subscript in these equations signifies that if the expression inside the bracket is greater than zero, then the rolling element at angular location θ_j is loaded giving rise to restoring force and if the expression inside the bracket is negative or zero, then the rolling element is not in the load zone, and restoring force is set to zero. For the balanced rotor condition, the unbalance force (F_u) is set to be zero.

The deformation of spring at inner race χ_j (from Fig. 2) can be obtained as

$$x_{\text{in}} + \chi_j \cos\theta_x = x_{\text{out}} + \rho_j \cos\theta_j, \tag{45}$$

$$y_{\text{in}} + \chi_j \sin\theta_x = y_{\text{out}} + \rho_j \sin\theta_j. \tag{46}$$

From these two equations, the expression for χ_j is obtained as

$$\chi_j = [(x_{\text{out}} - x_{\text{in}})^2 + \rho_j^2 + 2\rho_j(x_{\text{out}} - x_{\text{in}})\cos\theta_j + 2\rho_j(y_{\text{out}} - y_{\text{in}})\sin\theta_j + (y_{\text{out}} - y_{\text{in}})^2]^{1/2}. \tag{47}$$

Now the partial derivatives of χ_j with respect to ρ_j, x_{in} and y_{in} are

$$\frac{\partial \chi_j}{\partial \rho_j} = \frac{\rho_j + (x_{\text{out}} - x_{\text{in}})\cos\theta_j + (y_{\text{out}} - y_{\text{in}})\sin\theta_j}{\chi_j}, \tag{48}$$

$$\frac{\partial \chi_j}{\partial x_{\text{in}}} = \frac{(x_{\text{out}} - x_{\text{in}}) - \rho_j \cos\theta_j}{\chi_j}, \tag{49}$$

$$\frac{\partial \chi_j}{\partial y_{\text{in}}} = \frac{(y_{\text{out}} - y_{\text{in}}) - \rho_j \sin\theta_j}{\chi_j}. \tag{50}$$

The nonlinear stiffness associated with point contact of spring for the inner and outer races is calculated by using Eq. (12):

$$(k_{\text{in}}) = 7.055 \times 10^5[\{r + \rho_r + \Gamma\} - \chi_j]^{1/2}, \tag{51}$$

$$(k_{\text{out}}) = 7.055 \times 10^5[R - \{\rho_j + \rho_r + \Gamma\}]^{1/2}, \tag{52}$$

$$\frac{(\partial k_{\text{in}})}{\partial \rho_j} = -3.5725 \times 10^5[\{r + \rho_r + \Gamma\} - \chi_j]^{-1/2} \frac{\partial \chi_j}{\partial \rho_j}, \tag{53}$$

$$\frac{(\partial k_{\text{out}})}{\partial \rho_j} = 3.5725 \times 10^5[R - \{\rho_j + \rho_r + \Gamma\}]^{-1/2}. \tag{54}$$

2.5. BPF

When the shaft is rotating, applied loads are supported by a few balls restricted to a narrow load region and the radial position of the inner race with respect to the outer race depends on the elastic deflections at the ball to raceways contacts. Balls are deformed as they enter the loaded zone where the mutual convergence of the bearing races takes place and the balls rebound as they move to an unloaded region. Time taken by the shaft to regain its initial position is

$$t = \frac{\text{time for a complete rotation of cage}}{N_b}. \tag{55}$$

As the time needed for a complete rotation of the cage is $2\pi/\omega_c$, the shaft will be excited at the frequency of $(N_b \times \omega_c)$ known as BPF.

Hence, BPF (ω_{bp}) is

$$\omega_{\text{bp}} = \frac{1}{2} N_b\, \omega_{\text{inner}} \left[1 - \frac{\rho_j}{R_p}\right] + \frac{1}{2}\, N_b \omega_{\text{outer}} \left[1 + \frac{\rho_j}{R_p}\right]. \tag{56}$$

Vibrations associated with the BPF are known as BPV or the elastic compliance vibrations. The effect of BPF can be worst when it coincides with a natural frequency of the shaft-bearing system.

3. Results of the numerical simulations

The equations of motion (42–44) are solved using the modified Newmark-β method to obtain the radial displacement and velocity of the rolling elements. In order to eliminate the effect of the natural frequency, an artificial damping was introduced into the system. With this damping, transient vibrations are eliminated. Thus, peak steady-state amplitude of vibration can be measured. The longer the time to reach steady-state vibrations, the longer CPU time needed and hence the more expensive the computation. A value of $c = 200\,\text{Ns/m}$ was chosen. To observe the nonlinear behavior of the system, parameters of the ball bearing are selected and are shown in Table 2.

3.1. Initial conditions

The initial conditions and step size are very important for successful and economic computational solution. Particularly for nonlinear systems, different initial conditions mean a totally different system and hence different solutions. The larger the time step Δt, the faster the computation. On the other hand, the time step should be small enough to achieve an adequate accuracy. Also, very small time steps can increase the truncation errors. Therefore, an optimization should be made between them. The time step for the investigation is assumed as $\Delta t = 10^{-5}\,\text{s}$. At time $t = 0$ the following assumptions are made:

(i) The shaft is held at the center of the bearing and all balls are assumed to have equal axial preload.

(ii) The shaft is then given initial displacements and velocities. For fast convergence the initial displacements are set to the following values: $x_0 = 10^{-6}$ m and $y_0 = 10^{-6}$ m. The initial velocities are assumed to be zero: $\dot{x}_0 = 0$ and $\dot{y}_0 = 0$.

When $t \succ \Delta t$ the initial conditions have already passed and the normal procedure commences.

3.2. Cage run-out

The time history of the nonlinear responses has been examined for periodic behavior. This is done by examining the time series output, once per cycle, for sufficiently long segments of time step so that multiple periodic and aperiodic behaviors could be discerned from the post-transient solutions. Frequency spectra are generated for studying the stability and nature of solution. Aperiodic behavior in a deterministic dynamical system is characterized by broadband frequency spectra. In sub-synchronous frequencies the significant energy shows the aperiodic nature of the response. Due to the cage run-out, the rolling elements no longer stay equally spaced. Due to the non-uniform spacing, the BPF is modulated with the cage frequency. The resulting variation of the circumferential angle for a small run-out (Γ) is 0.01 μm.

Fig. 5 shows the vibrations for the bearing with a cage run-out having different numbers of balls. For a relatively small number of balls, the peak amplitudes of vibrations at BPF are more significant. Since, a small number of balls support the rotor, the natural frequency of the system is relatively low. When the number of balls is 3, the natural frequency coincides with the BPF ($\omega_{bp} = 102$ Hz) as shown in Fig. 5(a). The amplitude of the peak is 12 μm. Other major peaks at super-harmonics of vibration appear at an integral multiple of the BPF ($2\omega_{bp} = 204$ Hz, $3\omega_{bp} = 306$ Hz, $4\omega_{bp} = 408$ Hz). The BPF (ω_{bp}) and its harmonics character of the frequency spectra are also brought out by the phase plot with the closed orbits. For a system having 4 balls, the peak amplitude decreases and the natural frequency that coincides with BPF is pushed to a higher value of ($\omega_{bp} + \omega_c = 140$ Hz) as shown in Fig. 5(b). The amplitude of the peak is 10 μm. Other major peaks at super-harmonics of vibration appear at an integral multiple of the ball passage with cage frequency ($2\omega_{bp} + 2\omega_c = 280$ Hz, $3\omega_{bp} + 3\omega_c = 420$ Hz). The super-harmonic character of the frequency spectra is also confirmed by phase plot with its closed orbits.

For 5 balls, the peak amplitude of vibration appears in the spectrum at the BPF ($\omega_{bp} = 170$ Hz) as shown in Fig. 5(c). The amplitude of the peak is 4.2 μm. Other minor peaks appear at an integral multiple of the BPF ($2\omega_{bp} = 340$ Hz, $3\omega_{bp} = 510$ Hz). One peak at the developing stage appears where the BPF is modulated with the cage frequency, i.e. at $2\omega_{bp} + 3\omega_c = 442$ Hz. The closed loop of phase plot confirms the characteristics of the super-harmonic nature of frequency spectra. When the number of balls is 6, the peak amplitude of vibration appears in the spectrum at the BPF ($\omega_{bp} = 204$ Hz) as shown in Fig. 5(d). The amplitude of the peak is 2 μm. Other minor peaks appear at an integral multiple of the BPF ($2\omega_{bp} = 408$ Hz, $3\omega_{bp} = 612$ Hz). One peak appears where the BPF is modulated with the cage frequency, i.e. at $2\omega_{bp} + 2\omega_c = 476$ Hz. For 7 balls, the peak amplitude appears at the BPF ($\omega_{bp} = 238$ Hz) as shown in Fig. 5(e). The amplitude of the peak is 0.7 μm. Other minor peaks appear at an integral multiple of the BPF ($2\omega_{bp} = 476$ Hz, $3\omega_{bp} = 714$ Hz). One peak appears where the BPF is modulated with the cage frequency, i.e. at $2\omega_{bp} + \omega_c = 510$ Hz. For 8 balls, the peak amplitude of vibration appears at

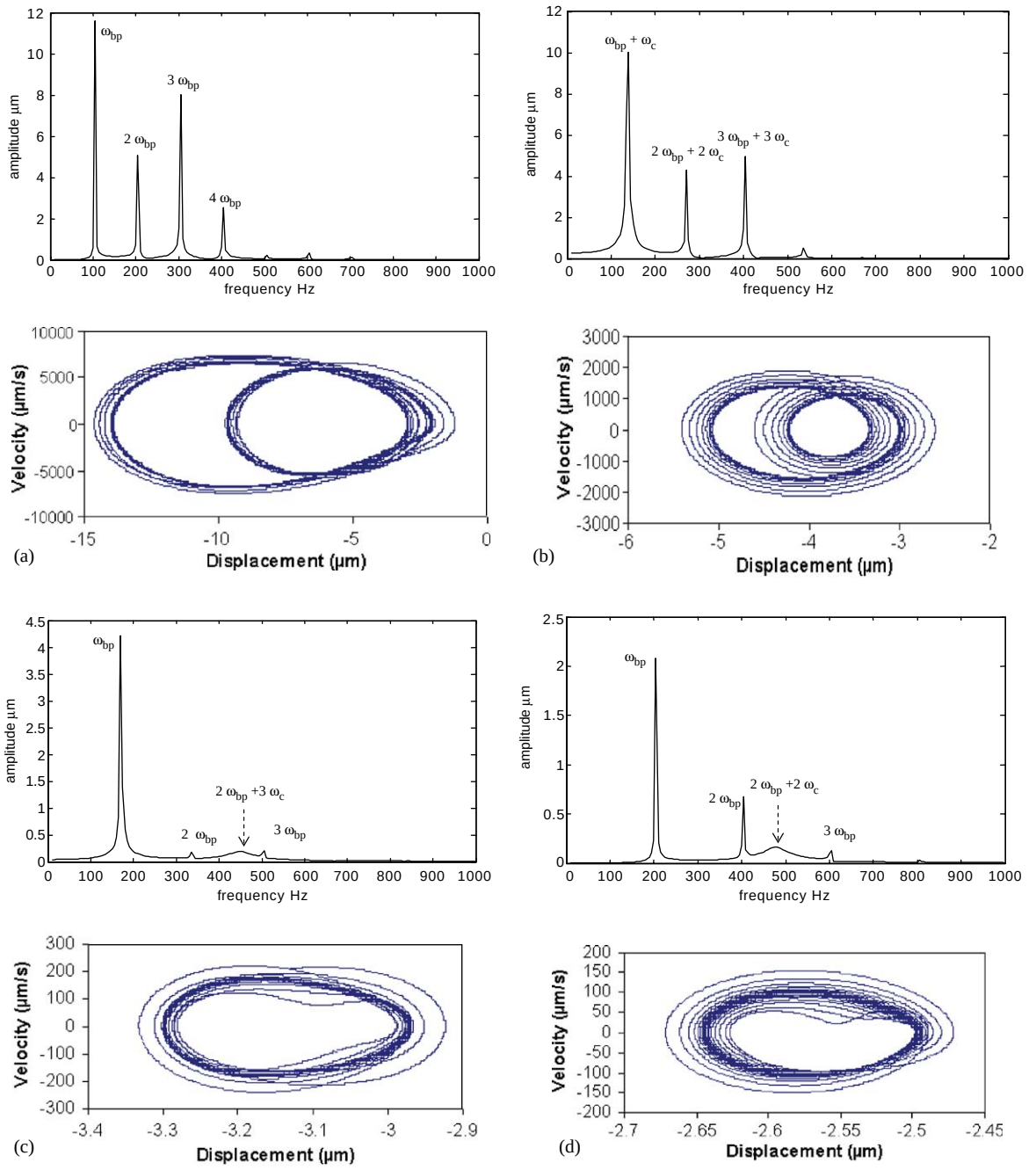

Fig. 5. (a) The FFT and phase plots due to cage run-out for $N_b = 3$. (b) The FFT and phase plots due to cage run-out for $N_b = 4$. (c) The FFT and phase plots due to cage run-out for $N_b = 5$. (d) The FFT and phase plots due to cage run-out for $N_b = 6$. (e) The FFT and phase plots due to cage run-out for $N_b = 7$. (f) The FFT and phase plots due to cage run-out for $N_b = 8$. (g) The FFT and phase plots due to cage run-out for $N_b = 9$. (h) The FFT and phase plots due to cage run-out for $N_b = 10$. (i) The FFT and phase plots due to cage run-out for $N_b = 11$. (j) The FFT and phase plots due to cage run-out for $N_b = 12$. (k) The FFT and phase plots due to cage run-out for $N_b = 13$. (l) The FFT and phase plots due to cage run-out for $N_b = 14$. (m) The FFT and phase plots due to cage run-out for $N_b = 15$. (n) The FFT and phase plots due to cage run-out for $N_b = 16$. (o) The FFT and phase plots due to cage run-out for $N_b = 17$.

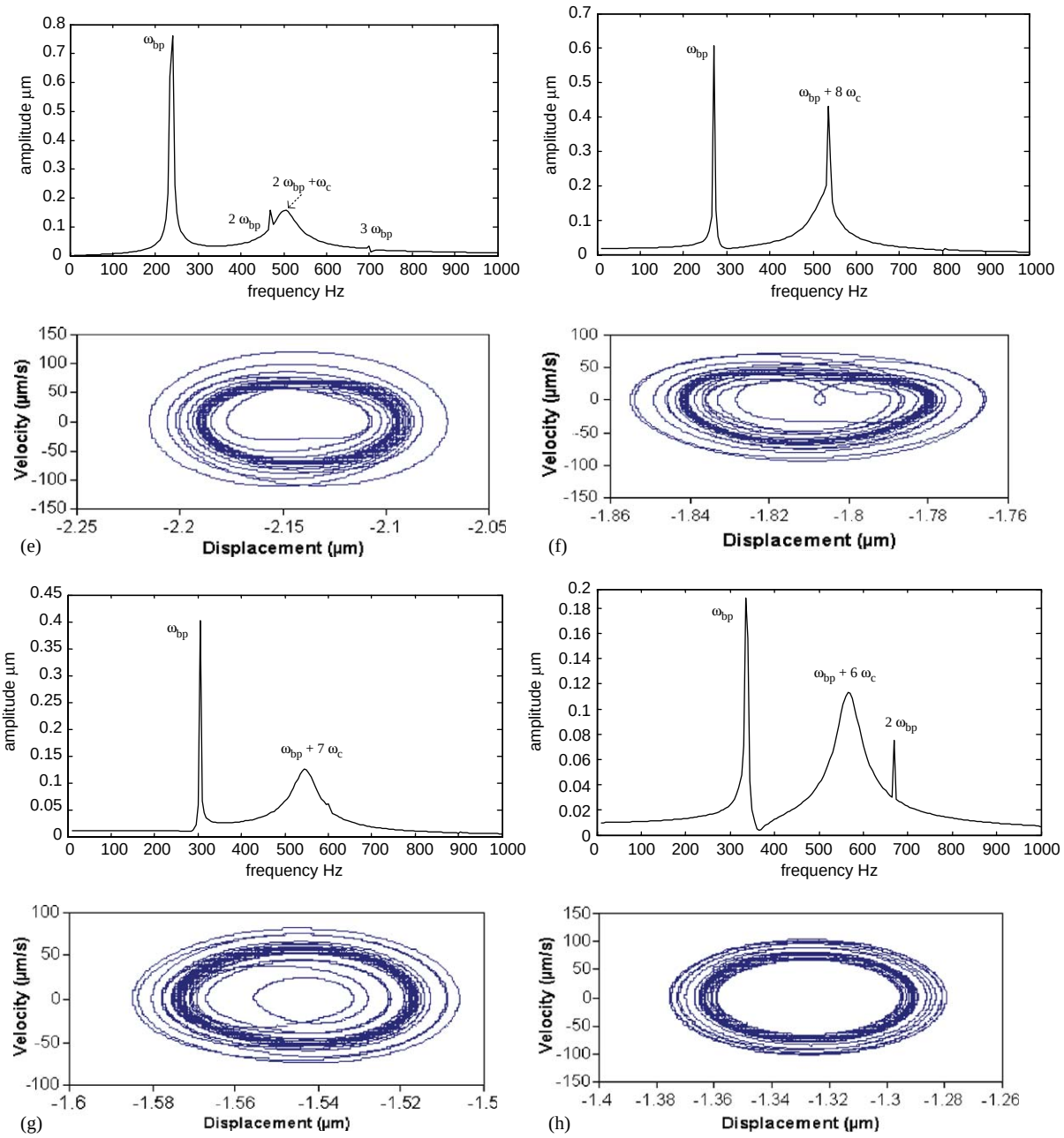

Fig. 5. (*Continued*)

($\omega_{bp} = 272$ Hz) as shown in Fig. 5(f). The amplitude of the peak is 0.6 µm. Other major peaks at super-harmonics of vibration appear at ($\omega_{bp} + 8\omega_c = 544$ Hz). Similarly, for 9–17 balls, the peak amplitudes of vibrations appear in the spectrum at an integer multiple of the number of balls and

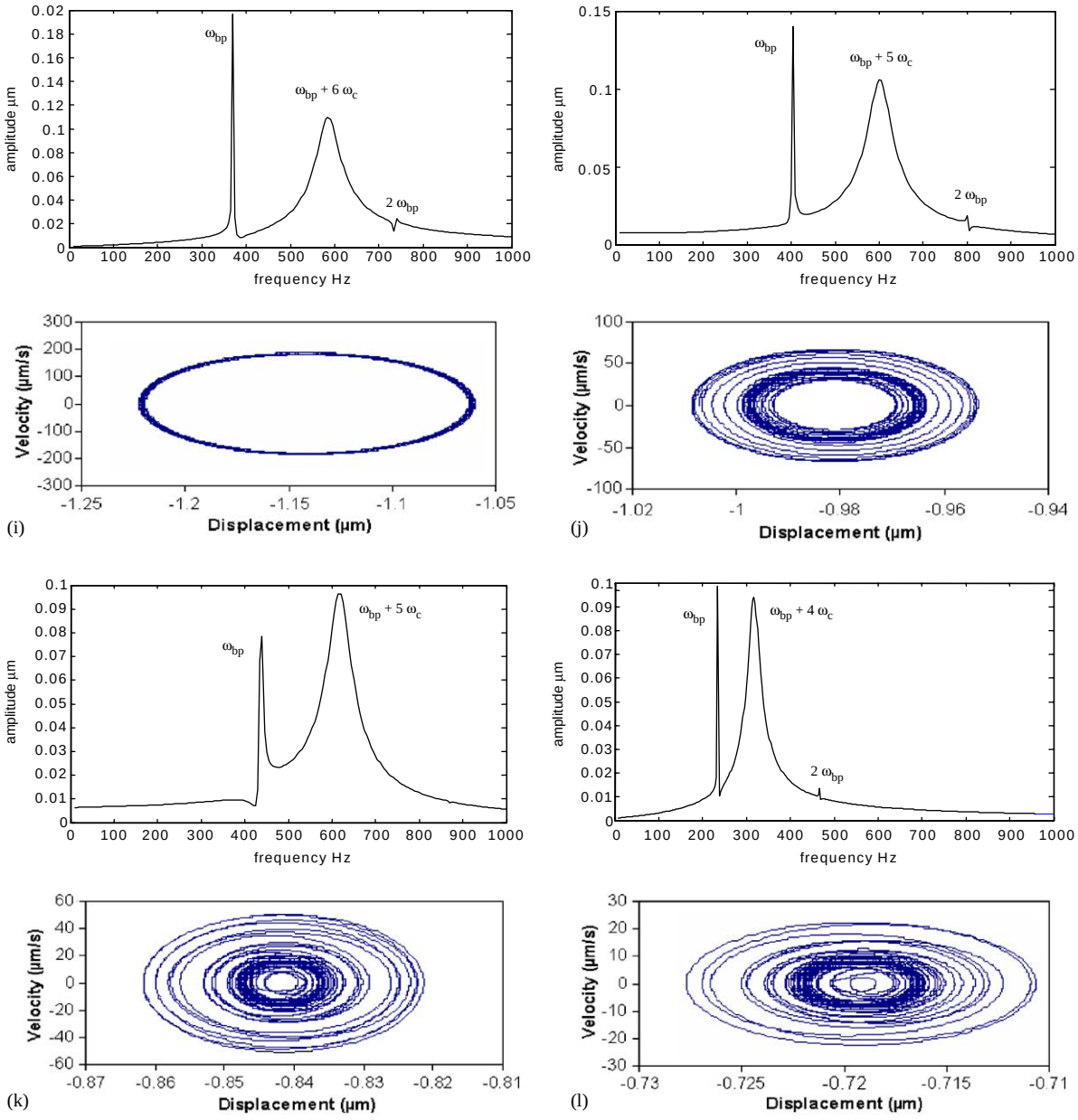

Fig. 5. (*Continued*)

the cage speed (BPF) as shown in Figs. 5(g)–(o). Other major peaks in these vibration spectrums are shown in Table 3.

When the number of balls is further increased, a peak at BPF always appears in the vibration spectrum but with relatively lower amplitude ($<0.5\,\mu m$), while the effects of super-harmonics

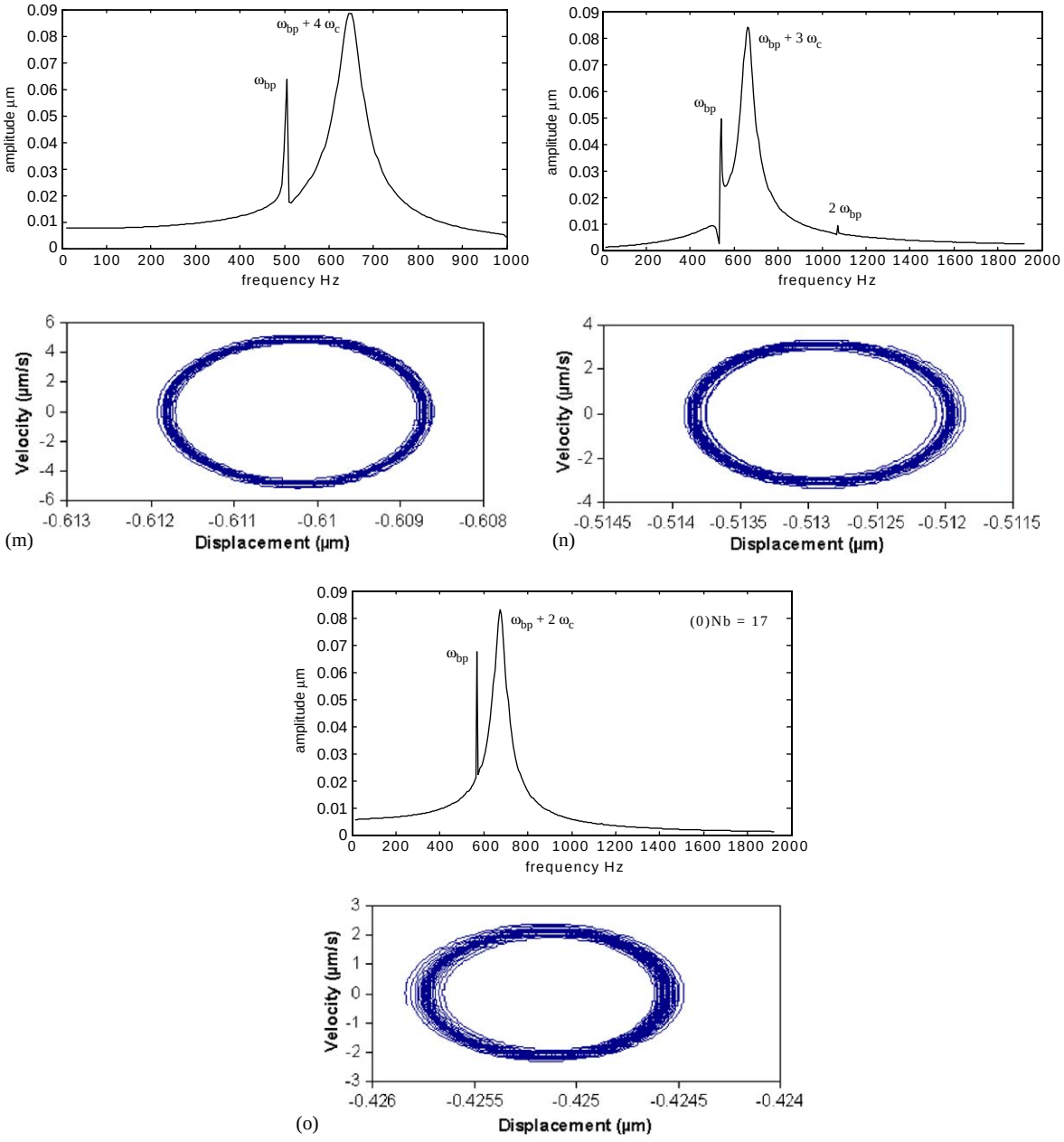

Fig. 5. (*Continued*)

disappear as the number of balls increases from 13 and onwards and the BPF appears at sub-harmonic in the vibration spectrum. All results show that cage run-out in the bearing due to the non-uniform spacing of the BPF is modulated with the cage frequency.

Table 3
Frequencies of the possible vibrations for different number of balls in a bearing due to cage run-out

Number of balls	Peak amplitude (magnitude)	Harmonic in bearing spectrum
3	ω_{bp} (12 μm)	$2\omega_{bp}$, $3\omega_{bp}$, $4\omega_{bp}$
4	$\omega_{bp} + \omega_c$ (10 μm)	$2\omega_{bp} + 2\omega_c$, $3\omega_{bp} + 3\omega_c$
5	ω_{bp} (4.2 μm)	$2\omega_{bp}$, $3\omega_{bp}$, $2\omega_{bp} + 3\omega_c$
6	ω_{bp} (2 μm)	$2\omega_{bp}$, $3\omega_{bp}$, $2\omega_{bp} + 2\omega_c$
7	ω_{bp} (0.8 μm)	$2\omega_{bp}$, $3\omega_{bp}$, $2\omega_{bp} + \omega_c$
8	ω_{bp} (0.6 μm)	$\omega_{bp} + 8\omega_c$
9	ω_{bp} (0.4 μm)	$\omega_{bp} + 7\omega_c$
10	ω_{bp} (0.19 μm)	$2\omega_{bp}$, $\omega_{bp} + 6\omega_c$
11	ω_{bp} (0.18 μm)	$2\omega_{bp}$, $\omega_{bp} + 6\omega_c$
12	ω_{bp} (0.14 μm)	$2\omega_{bp}$, $\omega_{bp} + 5\omega_c$
13	$\omega_{bp} + 5\omega_c$ (0.09 μm)	ω_{bp}
14	ω_{bp} (0.089 μm)	$2\omega_{bp}$, $\omega_{bp} + 4\omega_c$
15	$\omega_{bp} + 4\omega_c$ (0.088 μm)	ω_{bp}
16	$\omega_{bp} + 3\omega_c$ (0.085 μm)	ω_{bp}, $2\omega_{bp}$
17	$\omega_{bp} + 2\omega_c$ (0.084 μm)	ω_{bp}

4. Conclusion

In the present investigation, an analytical model of a rotor-bearing system has been developed to obtain the nonlinear vibration response due to cage run-out. In this paper, the nonlinear response of a perfectly rigid balanced rotor due to self-excited vibration in a ball bearing with small cage run-out is studied. The self-excited vibrations are due to varying compliance of the bearing, which arises because of the geometric and elastic characteristics of the bearing assembly varying according to cage position. Since the parametrically excited vibrations that occur irrespective of the quality and accuracy of the bearing are BPV (according to Sunnersjo [19]), the peak amplitude of vibrations that appear in the spectrum are at BPF. This is proved in the results of the presented article. The following conclusions are drawn from the obtained results:

(1) A single off-sized ball within a bearing produces vibrations at the cage speed. This is true for linear and nonlinear ball-to-race deflection coefficient.
(2) The highest axial vibrations due to cage run-out are at a speed of the number of balls times the cage speed, i.e. at the BPF, which is proved by Gad et al. [11] and Rahnejat and Gohar [12].
(3) Increasing the number of balls means increasing the number of balls supporting the rotor therefore increasing the system stiffness and reducing the vibration amplitude. This effect is exhibited in Fig. 5, which shows the phase plane diagram of the displacements for different numbers of balls when the rotor is released from an arbitrary position for free vibration without damping. When the number of balls is increased, the center of vibration approaches zero implying a stiffer system, which was theoretically proved by Aktürk et al. [13]. From this it can be predicted that the number of balls will reduce the effect of the BPF and because of the cage run-out, the modulating frequency dominant in the vibration spectrum.

(4) The number of balls in the bearings can be of importance in the rotor bearing dynamics and should be considered at the design stage.
(5) The highest axial vibrations due to cage run-out are at ($\omega = q\omega_{bp} \pm k\omega_c$ Hz). Hence, from this analysis the prediction about the major peaks at frequencies can be made for cage run-out with different number of balls.

References

[1] A.B. Jones, A general theory for elastically constrained ball and radial roller bearings under arbitrary load and speed conditions, *Journal of Basic Engineering* 82 (2) (1960) 309–320.
[2] T.A. Harris, *Rolling Bearing Analysis*, Willey, New York, 1991.
[3] A. Palmgren, *Ball and Roller Bearing Engineering*, SKF Industries Inc., 1959.
[4] C.T. Walters, The dynamics of ball bearings, *Journal of Lubricating Engineering* 93 (1971) 1–10.
[5] P.K. Gupta, The dynamics of rolling element bearings—part-III: ball bearing analysis, *Transactions of ASME* 101 (1979) 70.
[6] P.K. Gupta, *Advanced Dynamics of Rolling Element Bearings*, Springer, Berlin, 1984.
[7] J.W. Kennel, S.S. Bupara, A simplified model of cage motion in angular contact bearings operating in the EHD lubricating regime, *Journal of Lubricating Technology* 101 (1978) 395–401.
[8] C.R. Meeks, N. Foster, Computer simulation of ball bearing dynamics analytical predictions and test results, *Ball Bearing Symposium and Seminar*, Orlando, FL, March 9–12, 1987.
[9] C.R. Meeks, Ball bearing dynamic analysis using computer methods and correlation with empirical data, *International Tribology Conference*, Melbourne, Australia, December 2–4, 1987.
[10] C.R. Meeks, L. Tran, Ball bearing dynamic analysis using computer methods—part-I: analysis, *Journal of Tribology* 118 (1996) 52–58.
[11] E.H. Gad, S. Fukata, H. Tumara, Computer simulation of rotor radial vibration due to ball bearings, *Memories of the Faculties of Engineering, Kyushu Universities* 44 (1984) 83–111.
[12] H. Rahnejat, R. Gohar, The vibrations of radial ball bearings, *Proceedings of the Institution of Mechanical Engineers* 199 (C3) (1985) 181–193.
[13] N. Aktürk, M. Uneeb, R. Gohar, The effects of number of balls and preload on vibrations associated ball bearings, *Journal of Tribology* 119 (1997) 747–753.
[14] S.P. Harsha, K. Sandeep, R. Prakash, Nonlinear dynamic behaviors of rolling element bearings due to surface waviness, *Journal of Sound and Vibration* 272 (3–5) (2004) 557–580.
[15] S.P. Harsha, K. Sandeep, R. Prakash, Effects of preload and number of balls on nonlinear dynamic behaviors of ball bearing system, *International Journal of Nonlinear Sciences and Numerical Simulation* 4 (3) (2003) 265–278.
[16] S.P. Harsha, K. Sandeep, R. Prakash, The effect of speed of balanced rotor on nonlinear vibrations associated with ball bearings, *International Journal of Mechanical Sciences* 47 (4) (2003) 225–240.
[17] S.P. Harsha, Nonlinear dynamic response of a balanced rotor supported on rolling element bearings, *Mechanical Systems and Signal Processing* 19 (3) (2005) 551–578.
[18] K. Bathe, E. Wilson, *Numerical Methods in Finite Element Analysis*, Prentice-Hall, Englewood Cliffs, NJ, 1976.
[19] C.S. Sunnersjo, Varying compliance vibrations of rolling bearings, *Journal of Sound and Vibration* 58 (3) (1978) 363–373.